# Phase diagram of quark-antiquark and diquark condensates at finite temperature and density in the 3-dimensional Gross-Neveu model

Hiroaki Kohyama*

*Department of Physics, Osaka City University, Sumiyoshi-ku, Osaka 558-8585, Japan*

(Received 12 June 2007; published 11 February 2008)

We construct the phase diagrams of the quark-antiquark and diquark condensates at finite temperature and density in the 3-dimensional (3D) 2-flavor Gross-Neveu model. We found that, in contrast to the case of the 4D Nambu–Jona-Lasinio model, there is no region where the quark-antiquark and diquark condensates coexist. The phase diagrams obtained for some parameter region show similar structure with the 4D QCD phase diagram.

DOI: 10.1103/PhysRevD.77.045016 PACS numbers: 12.38.Aw, 11.10.Wx, 11.15.Pg, 12.38.Lg

## I. INTRODUCTION

The four-fermion interaction models are considered to be the effective theory for describing phase transitions. In $3+1$ dimensions (4D), the Nambu–Jona-Lasinio (NJL) model can be regarded as an effective theory of QCD [1]. The model successfully reproduces the chiral phase transition in quark matter (see, e.g. [2,3]). Furthermore, through recent studies of the diquark condensate, a variety of color superconducting phases are expected to be realized [4]. It has been shown that there is the region where the chiral (quark-antiquark) and diquark condensates coexist. (For a nice review, see, e.g. [5].)

The Gross-Neveu (GN) model proposed in 1974, is a model of Dirac fermions interacting via four-fermion interactions [6]. The 2D GN model is a renormalizable quantum field theory, and the 3D GN model is renormalizable in the leading $1/N$ order. They are closely related to the Bardeen-Cooper-Schrieffer theory of superconductivity [7]. Although the lower dimensional theory seems not to be realistic, the 2D GN type models are believed to be the effective models of 1-dimensional condensed matter systems such as conducting polymers like polyacetylene [8]. Since the GN model shares many properties with QCD, notably asymptotic freedom, chiral symmetry breaking in vacuum, the comparison of QCD, and the GN model is an interesting subject.

A variety of works have been devoted to the study of the GN model [9–16]. By using bag-model boundary conditions, a closed formula for the effective renormalized coupling constant in the large-$N$ limit, was derived in [10]. In a constant curvature space, the phase structure of chiral symmetry breaking in the GN model at finite temperature and density is discussed in [11]. The phase diagrams of the quark-antiquark condensate in the 2D GN model was obtained in [12]. In 3D, analyses so far have been done choosing 2-dimensional (2d) or 4-dimensional (4d) spinor representations for quarks. The case of the 2d representation is interesting itself because it is the nontrivial lowest-order representation. The phase diagram of the quark-antiquark condensate was constructed by employing the 2d representation in [13]. On the other hand in the case of the 4d representation, there exists the $\gamma^5$ (see, e.g. [17]) and the properties of the model bear resemblance to the NJL model in 4D. In this sense, this case is also interesting and the phase diagram of the quark-antiquark condensate was obtained in [14]. The relation between the 2d and 4d representations are discussed in [15]. Furthermore, through analyzing the 3D GN model with the 2d representation, the phase structure of the quark-antiquark($\bar{q}q$) and diquark($qq$) condensates in vacuum (zero temperature and chemical potential ($T=\mu=0$)) was studied in [16] under the condition that the $\bar{q}q$ and $qq$ condensates are much smaller than the cutoff scale of the model. It was found that the $\bar{q}q$ and $qq$ condensates do not coexist at $T=\mu=0$.

In this paper, we study the $\bar{q}q$ and $qq$ condensates at finite temperature and density in the 3D GN model with the 2d representation. We obtain the phase diagrams, and discuss the similarities and differences between the 3D GN model and the 4D NJL model.

The plan of the paper is as follows: In Sec. II we present the Lagrangian of the 3D GN model and introduce the mean-field approximation. In Sec. III we derive the thermodynamic potential. In Sec. IV we present the results of the numerical analyses. Among others, we show that there is no region where the $\bar{q}q$ and $qq$ condensates coexist. In Sec. V we display the phase diagrams. We find that the structure of phase diagrams bear resemblance to the QCD phase diagram for some parameter region. Section VI is devoted to summary and conclusions. In Appendixes A and B we describe the intermediate calculation and the renormalization for the thermodynamic potential.

## II. GROSS-NEVEU MODEL

The general form of the Lagrangian density of the 3D 2 flavor massless Gross-Neveu model with 2d representation reads

*kohyama@sci.osaka-cu.ac.jp

 

$$\mathcal{L} = \bar{q} i \not{\partial} q + G_S[(\bar{q}q)^2 + (\bar{q}\,\vec{\tau}\,q)^2] + G_D \sum_{a=1}^{8} (\bar{q}\,\vec{\tau}\,\lambda_a q^C)(\bar{q}^C \vec{\tau} \lambda_a q). \tag{1}$$

Here $\vec{\tau} = (\tau_1, \tau_2, \tau_3)$ are the Pauli matrices in flavor space and $\lambda_a$ is a Gell-Mann matrix in color space. $G_S$ and $G_D$ are the coupling constants of the $\bar{q}q$ and $qq$ interactions, respectively, and $C$ is the charge conjugation matrix. For the Dirac $\gamma$ matrices and $C$, we use the forms as in [16],

$$\gamma^0 = \begin{pmatrix} 1 & 0 \\ 0 & -1 \end{pmatrix}, \qquad \gamma^1 = \begin{pmatrix} 0 & i \\ i & 0 \end{pmatrix}, \qquad \gamma^2 = \begin{pmatrix} 0 & 1 \\ -1 & 0 \end{pmatrix} = C. \tag{2}$$

The charge conjugated field is defined by

$$q^C = C\bar{q}^T, \qquad \bar{q}^C = q^T C. \tag{3}$$

Following the reasonings described in [5], we reduce the Lagrangian density in Eq. (1) to

$$\mathcal{L} = \bar{q} i \not{\partial} q + G_S(\bar{q}q)^2 + \sum_{a=2,5,7} G_D(\bar{q}\tau_2\lambda_a q^C)(\bar{q}^C \tau_2 \lambda_a q). \tag{4}$$

$\mathcal{L}$ in Eq. (4) enjoys various symmetry properties, which are fully discussed in [16]. Here we choose a color direction for diquark condensate to blue, which is equivalent to select $\lambda_2$ in Eq. (4) (see [5]). Then we finally arrive at the following Lagrangian density:

$$\mathcal{L} = \bar{q} i \not{\partial} q + G_S(\bar{q}q)^2 + G_D(\bar{q}\tau_2\lambda_2 q^C)(\bar{q}^C \tau_2 \lambda_2 q). \tag{5}$$

Because of $\lambda_2$ in Eq. (5), only two colors (red, green) participate in the $qq$ condensate while all three colors (red, green, blue) do in the $\bar{q}q$ condensate.

Let us introduce the mean-field approximation and rewrite the Lagrangian density as follows:

$$\mathcal{L} = \bar{q} i \not{\partial} q - \bar{q}\sigma q - \frac{1}{2}\Delta^*(\bar{q}^C \tau_2 \lambda_2 q) - \frac{1}{2}\Delta(\bar{q}\tau_2\lambda_2 q^C) - \frac{\sigma^2}{4G_S} - \frac{|\Delta|^2}{4G_D}, \tag{6}$$

where $\sigma$ and $\Delta$ are the order parameters for the $\bar{q}q$ and $qq$ condensates:

$$\sigma = -2G_S\langle\bar{q}q\rangle \quad \text{and} \quad \Delta = -2G_D\langle\bar{q}^C\tau_2\lambda_2 q\rangle. \tag{7}$$

To deal with finite density system, we introduce a chemical potential being conjugate to the quark number $\bar{q}\gamma^0 q$. Then the Lagrangian density reads

$$\mathcal{L} = \bar{q} i \not{\partial} q + \bar{q}\mu\gamma^0 q - \bar{q}\sigma q - \frac{1}{2}\Delta^*(\bar{q}^C \tau_2 \lambda_2 q) - \frac{1}{2}\Delta(\bar{q}\tau_2\lambda_2 q^C) - \frac{\sigma^2}{4G_S} - \frac{|\Delta|^2}{4G_D}. \tag{8}$$

Introducing the Nambu-Gorkov basis [18]

$$\Psi = \begin{pmatrix} q \\ q^C \end{pmatrix} \quad \text{and} \quad \bar{\Psi} = (\bar{q}\bar{q}^C),$$

and using the relation $\bar{q}^C\gamma^0 q^C = -\bar{q}\gamma^0 q$, we can write the Lagrangian density in a momentum space as

$$\mathcal{L} = \frac{1}{2}\bar{\Psi}G^{-1}\Psi - \frac{\sigma^2}{4G_S} - \frac{|\Delta|^2}{4G_D}, \tag{9}$$

where

$$G^{-1} = \begin{pmatrix} (\not{p} - \sigma + \mu\gamma^0)\mathbf{1}_f\mathbf{1}_c & -\tau_2\lambda_2\Delta\mathbf{1}_s \\ -\tau_2\lambda_2\Delta^*\mathbf{1}_s & (p - \sigma - \mu\gamma^0)\mathbf{1}_f\mathbf{1}_c \end{pmatrix}. \tag{10}$$

$\mathbf{1}_f$, $\mathbf{1}_c$, and $\mathbf{1}_s$ are the unit matrix in flavor, color, and spinor space, respectively.

## III. THE THERMODYNAMIC POTENTIAL

### A. Derivation of the thermodynamic potential

Following the standard method, we can evaluate the thermodynamic potential:

$$\Omega(\sigma, |\Delta|) = \frac{\sigma^2}{4G_S} + \frac{|\Delta|^2}{4G_D} - \frac{1}{\beta V}\ln\int[d\Psi] \times \exp\left[\frac{1}{2}\sum_{n,\boldsymbol{p}}\bar{\Psi}(\beta G^{-1})\Psi\right], \tag{11}$$

where $\beta = 1/T$ is the inverse temperature and $V$ is the volume of the system. With the help of the formula

$$\int[d\Psi]\exp\left[\frac{1}{2}\sum_{n,\boldsymbol{p}}\bar{\Psi}(\beta G^{-1})\Psi\right] = \det{}^{1/2}(\beta G^{-1}), \tag{12}$$

we can rewrite Eq. (11) as

$$\Omega(\sigma, |\Delta|) = \frac{\sigma^2}{4G_S} + \frac{|\Delta|^2}{4G_D} - \frac{1}{\beta V}\ln\det{}^{1/2}(\beta G^{-1}). \tag{13}$$

After some manipulation which is given in Appendix A, the determinant becomes

$$\det{}^{1/2}(G^{-1}) = [p_0^2 - E_\Delta^{+2}]^2[p_0^2 - E_\Delta^{-2}]^2[p_0^2 - E^{+2}] \times [p_0^2 - E^{-2}], \tag{14}$$

where $p_0 = i(2n+1)\pi T$, $(n = \cdots, -2, -1, 0, 1, 2, \cdots)$ and

$$E^\pm \equiv E \pm \mu, \qquad E \equiv \sqrt{\vec{p}^2 + \sigma^2}, \qquad \vec{p}^2 = p_1^2 + p_2^2,$$
$$E_\Delta^{\pm 2} \equiv E^2 + \mu^2 + |\Delta|^2 \pm 2\sqrt{E^2\mu^2 + \sigma^2|\Delta|^2}(\geq 0). \tag{15}$$

Thus, we obtain

$$\Omega(\sigma,|\Delta|) = \frac{\sigma^2}{4G_S} + \frac{|\Delta|^2}{4G_D} - T\sum_{\pm}\sum_{n}\int\frac{d^2p}{(2\pi)^2}[\ln[\beta^2(p_0^2 - E^{\pm 2})] + 2\ln[\beta^2(p_0^2 - E_\Delta^{\pm 2})]]. \quad (16)$$

The frequency summation may be performed in a standard manner [19]:

$$\sum_n \ln[\beta^2(p_0^2 - E^2)] = \beta[E + 2T\ln(1 + e^{-\beta E})]. \quad (17)$$

Then we finally obtain

$$\Omega(\sigma,|\Delta|) = \Omega_0(\sigma,|\Delta|) + \Omega_T(\sigma,|\Delta|), \quad (18)$$

$$\Omega_0(\sigma,|\Delta|) = \frac{\sigma^2}{4G_S} + \frac{|\Delta|^2}{4G_D} - 2\int\frac{d^2p}{(2\pi)^2}[E + E_\Delta^+ + E_\Delta^-], \quad (19)$$

$$\Omega_T(\sigma,|\Delta|) = -2T\sum_{\pm}\int\frac{d^2p}{(2\pi)^2}[\ln(1 + e^{-\beta E^{\pm}}) + 2\ln(1 + e^{-\beta E_\Delta^{\pm}})]. \quad (20)$$

Here $\Omega_0$ is $T$ independent contribution, which is ultraviolet divergent, while the temperature dependent part $\Omega_T$ is finite. For the purpose of later use, we write $\Omega_0$, in Eq. (19), in the integral form in the 3D Euclidean momentum space,

$$\Omega_0(\sigma,|\Delta|) = \frac{\sigma^2}{4G_S} + \frac{|\Delta|^2}{4G_D} - \sum_{\pm}\int\frac{d^3p_E}{(2\pi)^3}\left[\ln\left(\frac{p_{E0}^2 + E^{\pm 2}}{p_E^2}\right) + 2\ln\left(\frac{p_{E0}^2 + E_\Delta^{\pm 2}}{p_E^2}\right)\right]. \quad (21)$$

The $p_E^2$ terms in the denominators in the second line of Eq. (21) are inserted so as to drop an irrelevant infinite constant.

### B. Renormalized thermodynamic potential

As mentioned in the previous subsection, $\Omega_0$, $T$ independent part of $\Omega$ is ultraviolet divergent. To eliminate the divergences, we introduce the counter Lagrangian as derived in [13] (see also [6]):

$$\mathcal{L}_C = -\tfrac{1}{2}Z_S\sigma^2 - Z_D|\Delta|^2, \quad (22)$$

$$Z_S = \frac{6}{\pi^2}\Lambda - \frac{3}{4}\alpha, \qquad Z_D = \frac{2}{\pi^2}\Lambda - \frac{1}{4}\alpha, \quad (23)$$

where $\Lambda$ is the 3D momentum cutoff and $\alpha$ is the arbitrary renormalization scale. For completeness, the derivation of Eq. (23) is given in Appendix B.

Introducing the above counter Lagrangian, $\Omega_0$ in Eq. (21) turns out to be finite and the renormalized $\Omega_{0r}$ becomes

$$\Omega_{0r}(\sigma,|\Delta|) = \left(\frac{1}{4G_S} - \frac{3}{8}\alpha\right)\sigma^2 + \left(\frac{1}{4G_D} - \frac{1}{4}\alpha\right)|\Delta|^2 - \sum_{\pm}\int\frac{d^3p_E}{(2\pi)^3}\left[\ln\left(\frac{p_{E0}^2 + E^{\pm 2}}{p_E^2}\right) + 2\ln\left(\frac{p_{E0}^2 + E_\Delta^{\pm 2}}{p_E^2}\right) - \frac{3}{p_E^2}\sigma^2 - \frac{2}{p_E^2}|\Delta|^2\right]. \quad (24)$$

Note that the counterterms cancel the divergences and the integral becomes finite. Thus, after performing the renormalization, the renormalized thermodynamic potential $\Omega_r(\equiv \Omega_{0r} + \Omega_T)$ is finite and we carry out the numerical analyses on $\Omega_r$.

Before studying the $\bar{q}q$ and $qq$ condensates, we rewrite $\Omega_r$ by using the following parameters:

$$\sigma_0 \equiv -\frac{2\pi}{3}\left(\frac{1}{4G_S} - \frac{3}{8}\alpha\right), \quad (25)$$

$$\Delta_0 \equiv -\pi\left(\frac{1}{4G_D} - \frac{1}{4}\alpha\right). \quad (26)$$

Using $\sigma_0$ and $\Delta_0$, we can write $\Omega_r$ at $T = 0 = \mu$ as

$$\Omega_r(\sigma,|\Delta|)|_{T=0=\mu} = -\frac{3}{2\pi}\sigma_0\sigma^2 - \frac{1}{\pi}\Delta_0|\Delta|^2 + \frac{1}{3\pi}\sigma^3 + \frac{1}{3\pi}(\sigma + |\Delta|)^3 + \frac{1}{3\pi}|\sigma - \Delta|^3. \quad (27)$$

Throughout in the following, we use the parameters $\sigma_0$ and $\Delta_0$. By minimizing Eq. (27) for $\Delta = 0$, one can easily verify that, when $\sigma_0 > 0$, $\sigma_0$ corresponds to the $\bar{q}q$ condensate in vacuum.

## IV. QUARK-ANTIQUARK AND DIQUARK CONDENSATES

We have obtained the thermodynamic potential in the previous section. Equations (24)–(26) tell us that this model has two free parameters $(\sigma_0, \Delta_0)$. In this paper, we aim to study the system where the $\bar{q}q$ condensate always takes place in vacuum if $\Delta = 0$, so we assume $\sigma_0$ to be positive (see, e.g. [12]). After fixing $\sigma_0$, there remains a free parameter $\Delta_0$ and we introduce $r$ through

$$r \equiv \Delta_0/\sigma_0. \quad (28)$$

There is no direct way of fixing the parameter $r$, and we analyze for different $r$'s.

Figure 1 plots the $\bar{q}q$ and $qq$ condensates (normalized by $\sigma_0$) at $T = 0$. In the case of $r = -10$ (panel (a)), we see that the $\bar{q}q$ condensate disappears at $\mu = 1.0\sigma_0$, and there

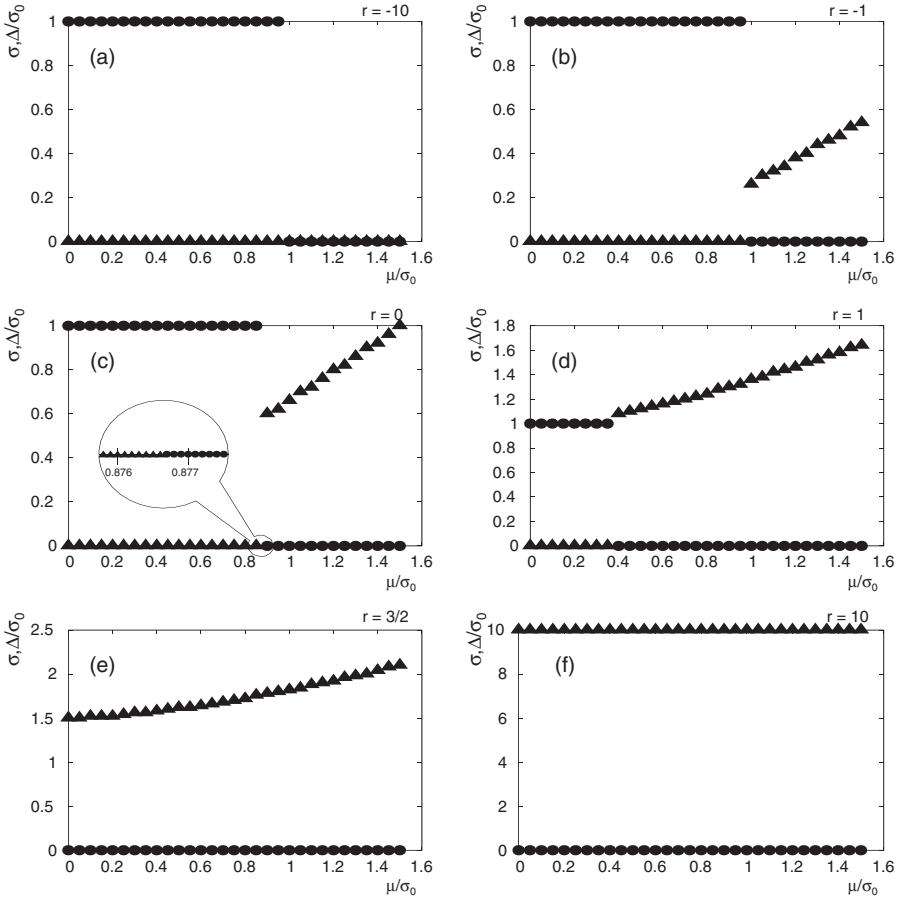


FIG. 1. $\sigma$ (circles) and $\Delta$ (triangles) as a function of chemical potential $\mu$ at $T = 0$.

does not arise the $qq$ condensate. Through numerical analyses, we have found that this is the case for $r < -6.3$. On the other hand for $r = -1$ (panel (b)), at $\mu = 1.0\sigma_0$ the $\bar{q}q$ condensate disappears and at the same time, the $qq$ condensate arises. Similar results are obtained for $r = 0$ and 1, where the transition densities are $\mu = 0.88\sigma_0$ and $\mu = 0.4\sigma_0$, respectively. All the phase transitions in the panels (a)–(d) are of the first order. With increasing the ratio $r$, the $qq$ condensate $\Delta$ becomes larger and eventually exceeds the $\bar{q}q$ condensate at $\mu = 0$. As seen from the panel (e) for $r = 3/2$, the $\bar{q}q$ condensate disappears and only the $qq$ condensate exists for whole $\mu$. More detailed analyses show that the $\bar{q}q$ condensate does not occur for $r > 1.15$. Thus the results are sensitive to the ratio $r = \Delta_0/\sigma_0$. It should be emphasized that there is no region where the $\bar{q}q$ and $qq$ condensates coexist. To clarify this fact, we show the close-up of the condensates near the phase transition point in Fig. 1(c).

Now we turn to the $T \neq 0$ case. We display the results for $(r, T) = (-1, 0.1\sigma_0)$ and $(-1, 0.4\sigma_0)$ in Fig. 2. These panels show that the $\bar{q}q$ condensate for $\mu = 0$ is $1.0\sigma_0$ at $T = 0.1\sigma_0$ and $0.92\sigma_0$ at $T = 0.4\sigma_0$. The $qq$ condensate for $\mu = 1.0\sigma_0$ is $0.24\sigma_0$ at $T = 0.1\sigma_0$ and 0 at $T = 0.4\sigma_0$. Thus, as $T$ increases, the $\bar{q}q$ and $qq$ condensates decrease.

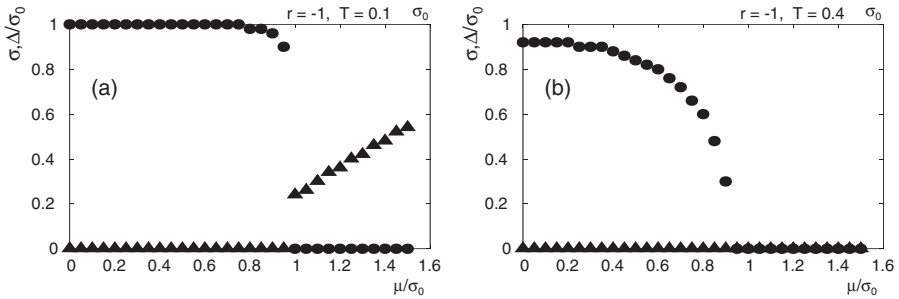


FIG. 2. The two gaps $\sigma$ (circles) and $\Delta$ (triangles) for $(r, T) = (-1, 0.1\sigma_0)$ and $(-1, 0.4\sigma_0)$.

Note that the $qq$ condensate appears at $T = 0.1\sigma_0$ and does not appear at $T = 0.4\sigma_0$, which indicates that $\Delta$ disappears at high temperature. A more detailed analysis shows that the $qq$ condensate at $\mu = 1.0\sigma_0$ disappears for $T > 0.15\sigma_0$ (see Sec. V). It should be noted that, within our numerical accuracy, there is no region where the $\bar{q}q$ and $qq$ condensates coexist, also at finite temperature. The results for other values of $r$ are qualitatively the same. As the temperature increases, the condensates become smaller and completely disappear at the critical temperature. This is the signal of the phase transition from the condensate state to the normal state.

From Fig. 2, we see that the phase transition for $T = 0.1\sigma_0$ is apparently of the first order and the case for $T = 0.4\sigma_0$, it is of the second order. Investigating the thermodynamic potential as a function of the $\bar{q}q$ condensate as in [12], we have confirmed this fact. We will discuss the phase transition and its order in the next section in more detail.

## V. THE PHASE DIAGRAM

Through minimizing the thermodynamic potential, one obtains the phase diagram. In Fig. 3, we display the phase diagrams for various values of $r$. For $r < -6.3$, there appears the pure $\bar{q}q$ condensate phase at low temperature and density and no $qq$ condensate phase appears. In the cases of $r = -1, 0$ the phase diagrams bear resemblance to that of QCD. For $r = -1$ with $T = 0$, the phase transition from the $\bar{q}q$ condensate phase to the $qq$ condensate phase takes place at $\mu \simeq 0.98\sigma_0$. For $\mu = 0$, as $T$ increases, the transition from the $\bar{q}q$ condensate phase to the normal phase takes place at $T \simeq 0.73\sigma_0$, which applies also for $r = -10, 0, 1$. On the other hand, in the cases of $r = 3/2$ and 10, the transition temperature for $\mu = 0$ are $T \simeq 1.08\sigma_0$ and $10\sigma_0$, respectively.

As $r$ increases, the region of $\bar{q}q$ condensate phase shrinks toward the $\mu$ axis and the region of the $qq$ condensate phase increases toward the $T$ axis. For $r = 3/2$ and 10, the $\bar{q}q$ condensate does not exist only and the $qq$ condensate appears. Through numerical analysis, we have found that the $\bar{q}q$ condensate phase disappears completely at $r \simeq 1.15$.

The points $(\mu_c, T_c)$ shown in the panel (a), (b), and (c) in Fig. 3 represent the critical points from the first order phase transition to the second order. The phase transition below the critical temperature $T_c$ is the first order and above $T_c$ is the second order. On the other hand in the panel (d), there is no critical point and the phase transition from $\bar{q}q$ condensate to the $qq$ condensate is always the first order. The more detailed analysis tells us that the critical point disappears for $r \simeq 1$, and it always appears between the $\bar{q}q$ phase and the normal phase. With respect to the $qq$ condensate, the

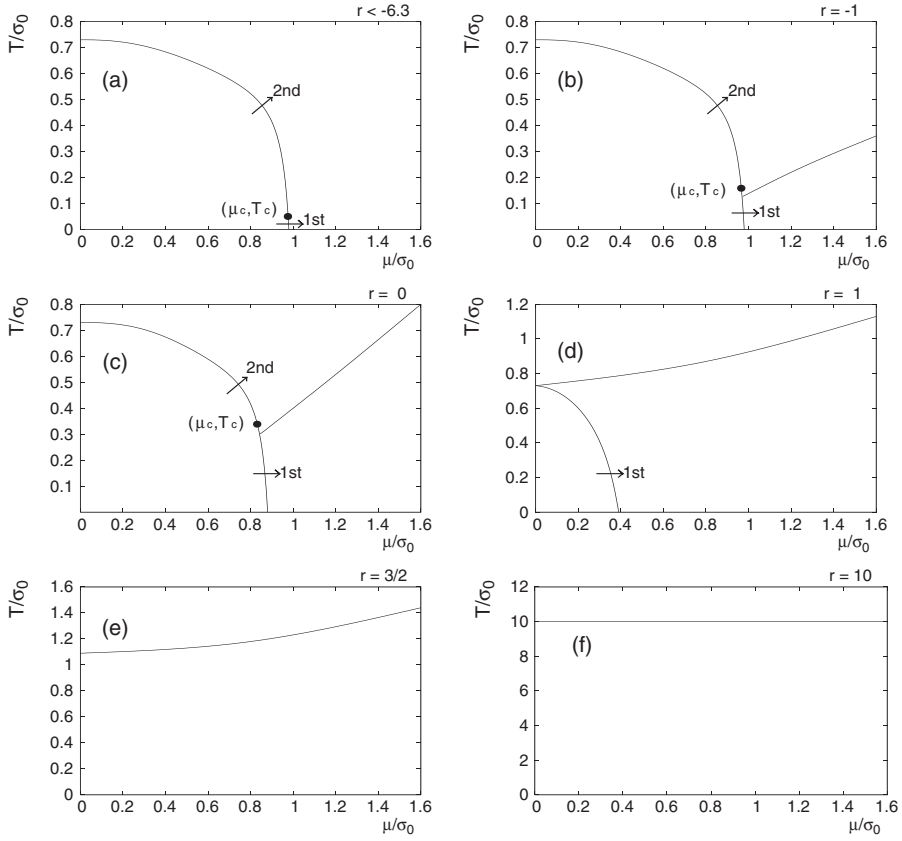


FIG. 3. The phase diagram of the 3D GN model.

phase transition from the $qq$ to the normal phase is always of the second order.

## VI. SUMMARY AND CONCLUSIONS

We have studied the $\bar{q}q$ and $qq$ condensates in the 3D GN model with 2d spinor quarks, and obtained the phase diagram for various values of $r = \Delta_0/\sigma_0$.

We have found that the behaviors of the $\bar{q}q$ and $qq$ condensates at $T = 0$, in Fig. 1, bear resemblance to that of the 4D NJL model [5]: With increasing $r$, the $qq$ condensate becomes more dominant and the $\bar{q}q$ condensate disappears completely for $r > 1.15$.

Figures 1 and 2 show that, both for $T = 0$ and $T \neq 0$, there is no region where the $\bar{q}q$ and $qq$ condensates coexist. This is a characteristic feature in the 3D GN model which does not happen in the 4D NJL model.

From Figs. 3(b) and 3(c), we see that for $r = -1$, 0, there is a close resemblance between the phase diagrams for $r = -1$, 0 and that of QCD. The $\bar{q}q$ condensate phase here corresponds to the hadronic phase in QCD, and the $qq$ condensate phase corresponds to the color superconducting phase. In the case for $r < -6.3$, there does not appear the $qq$ condensate phase, and the phase diagram shows close similarity with the QCD phase diagram without the color superconducting phase. However the diagrams for $r = 1$, $3/2$, and 10 are very different from the QCD case. Especially when $r = 3/2$ and 10, there is no $\bar{q}q$ condensate and only the $qq$ condensate exists.

The circles in Fig. 3 indicate the critical points with respect to the $\bar{q}q$ phase transition from first order to the second order. Note that the phase transition from the $\bar{q}q$ condensate to the $qq$ condensate is always of the first order. As seen from Figs. 1 and 2, when the $qq$ condensate arises, the $\bar{q}q$ condensate disappears rapidly.

We have found that the phase structure drastically changes according to the value $r = \Delta_0/\sigma_0$. With increasing $r$, the $qq$ condensate becomes larger. This means that the $qq$ condensate becomes more dominant when $\Delta_0$ increases. On the other hand, $\Delta_0$ is related to the $qq$ coupling constant $G_D$ through Eq. (26), and as $\Delta_0$ increases, $G_D$ increases. In the same reason, when $G_S$ increases (decreases), $\sigma_0$ becomes large (small), which causes $r$ to decrease (increase). With these observations in mind, we can conclude that when $G_D$ is small, the $\bar{q}q$ condensate is dominant over the $qq$ condensate, and the $qq$ condensate becomes larger when $G_D$ increases. This is the same phenomenon as seen in the 4D NJL model.

Finally it should be mentioned again that we have found the absence of the coexisting phase in the 3D GN model *with 2d spinor quarks*. As mentioned in Sec. I, the 3D GN model with 4d spinor quarks bears resemblance to the 4D NJL model. Then it is worth studying the phase diagram in the 3D GN model with 4d spinor representation to see whether the coexisting phase appears as in the 4D NJL model or does not appear as in the present case.

## ACKNOWLEDGMENTS

I would like to express my sincere gratitude to A. Niegawa and M. Inui for useful discussions.

## APPENDIX A: THE DERIVATION OF EQ. (14)

The determinant of $G^{-1}$ can be rewritten as

$$\det G^{-1} = \det\begin{pmatrix} (\not{p} - \sigma + \mu\gamma^0)\mathbf{1}_f\tilde{\mathbf{1}}_c & i\epsilon\tau_2\Delta\mathbf{1}_s \\ i\epsilon\tau_2\Delta^*\mathbf{1}_s & (\not{p} - \sigma - \mu\gamma^0)\mathbf{1}_f\tilde{\mathbf{1}}_c \end{pmatrix} \times \det\begin{pmatrix} (\not{p} - \sigma + \mu\gamma^0)\mathbf{1}_f & 0 \\ 0 & (\not{p} - \sigma - \mu\gamma^0)\mathbf{1}_f \end{pmatrix}, \tag{A1}$$

where $\tilde{\mathbf{1}}_c$ is the unit matrix and $\epsilon$ is the antisymmetric matrix in color (red and green) space, $\epsilon_{rg} = -\epsilon_{gr} = 1$. For a $2 \times 2$ block matrix with matrices $A$, $B$, $C$, and $D$, we have the identity

$$\det\begin{pmatrix} A & B \\ C & D \end{pmatrix} = \det(-CB + CAC^{-1}D). \tag{A2}$$

Replacing $A$, $B$, $C$, and $D$ with corresponding elements in the first line of Eq. (A1), we get

$$\begin{aligned} &\det\begin{pmatrix} (\not{p} - \sigma + \mu\gamma^0)\mathbf{1}_f\tilde{\mathbf{1}}_c & i\epsilon\tau_2\Delta\mathbf{1}_s \\ i\epsilon\tau_2\Delta^*\mathbf{1}_s & (\not{p} - \sigma - \mu\gamma^0)\mathbf{1}_f\tilde{\mathbf{1}}_c \end{pmatrix} \\ &= \det(-|\Delta|^2 + p_0^2 - \vec{p}^2 + \sigma^2 - \mu^2 - 2\sigma\not{p} \\ &\quad - \mu\not{p}\gamma^0 + \mu\gamma^0\not{p})^4 \\ &= (p_0^2 - E^2 - \mu^2 - |\Delta|^2 - 2\sqrt{E^2\mu^2 + \sigma^2|\Delta|^2})^4 \\ &\quad \times (p_0^2 - E^2 - \mu^2 - |\Delta|^2 + 2\sqrt{E^2\mu^2 + \sigma^2|\Delta|^2})^4, \end{aligned} \tag{A3}$$

which leads to the first two factors in Eq. (14). After calculating the second line of Eq. (A1), we finally obtain $\Omega(\sigma, |\Delta|)$ in Eq. (14).

## APPENDIX B: RENORMALIZATION IN VACUUM

As mentioned in Sec. I, the standard $O(N)$ 3D GN model is renormalizable in the leading $1/N$ order. This is also the case for the thermodynamic potential equation (16) in the present model within the mean-field approximation.

Following the procedure as in [13] (see also [6]), we carry out the renormalization and obtain the renormalized thermodynamic potential.

The divergent part of the potential is $\Omega_0$ in Eq. (21) and the divergent integral is written as

$$\Omega_{0\mathrm{div}}(\sigma, |\Delta|) = -\frac{3}{\pi^2}\sigma^2\Lambda - \frac{2}{\pi^2}|\Delta|^2\Lambda. \tag{B1}$$

It is to be noted that $\Omega_{0\mathrm{div}}$ is independent of $\mu$.

To eliminate this divergence, we introduce the counter Lagrangian $\mathcal{L}_C$, Eq. (22). For determining $Z_S$ in $\mathcal{L}_C$, we consider the one-loop radiative correction to the $\sigma$ propagator in the 2 + 1 Minkowski momentum space as calculated in [13],

$$D_\sigma(p^2) = \frac{-i}{(1/2G_S) + i\Pi(p^2)}, \tag{B2}$$

$$\Pi(p^2) = -N_f N_c \int \frac{d^3k}{(2\pi)^3} \frac{\mathrm{Tr}[\not{k}(\not{k} - \not{p})]}{k^2(k-p)^2}, \tag{B3}$$

where $N_f$ and $N_c$ are the numbers of flavors and colors. $\Pi(p^2)$ shown above is ultraviolet divergent, and the counterterm $Z_S$ is introduced so as to eliminate its divergent contribution. Here we employ the renormalization condition

$$D_\sigma(p^2) = -2iG_S, \quad \text{at } p_0^2 - \vec{p}^2 = -\alpha^2. \tag{B4}$$

This means that the counterterm $Z_S$ should satisfy the following relation

$$Z_S = -i\Pi(p^2)|_{p_0^2 - \vec{p}^2 = -\alpha^2}, \tag{B5}$$

going into the Euclidean space, and restricting the integration region with a sphere of radius $\Lambda$. Then after evaluating the integral equation (B3) and using the condition equation (B5), we obtain

$$Z_S = \frac{6}{\pi^2}\Lambda - \frac{3}{4}\alpha. \tag{B6}$$

In a similar manner, one obtains the renormalization constant $Z_D$:

$$Z_D = \frac{2}{\pi^2}\Lambda - \frac{1}{4}\alpha. \tag{B7}$$

Introduction of the counter Lagrangian $\mathcal{L}_C$ eliminates $\Omega_{0\mathrm{div}}$, and we obtain the renormalized $\Omega_{0r}$.


[1] Y. Nambu and G. Jona-Lasinio, Phys. Rev. **122**, 345 (1961); **124**, 246 (1961).
[2] Tetsuo Hatsuda and Teiji Kunihiro, Phys. Rep. **247**, 221 (1994).
[3] T. M. Schwarz, S. P. Klevansky, and G. Papp, Phys. Rev. C **60**, 055205 (1999); F. Gastineau, R. Nebauer, and J. Aichelin, Phys. Rev. C **65**, 045204 (2002); M. Buballa, J. Hosek, and M. Oertel, Phys. Rev. D **65**, 014018 (2001); D. Ebert, K. G. Klimenko, and H. Toki, Phys. Rev. D **64**, 014038 (2001); Michael Buballa, Phys. Rep. **407**, 205 (2005).
[4] Mark Alford, Annu. Rev. Nucl. Part. Sci. **51**, 131 (2001).
[5] Mei Huang, Int. J. Mod. Phys. E **14**, 675 (2005).
[6] D. J. Gross and A. Neveu, Phys. Rev. D **10**, 3235 (1974).
[7] J. Bardeen, L. N. Cooper, and J. R. Schrieffer, Phys. Rev. **106**, 162 (1957); **108**, 1175 (1957).
[8] M. Thies and K. Urlichs, Phys. Rev. D **72**, 105008 (2005).
[9] S. Weinberg, Phys. Rev. D **56**, 2303 (1997); B. Charneski, A. F. Ferrari, and M. Gomes, J. Phys. A **40**, 3633 (2007); J. Feinberg and S. Hillel, J. Phys. A **39**, 6341 (2006).
[10] A. P. C. Malbouisson, J. M. C. Malbouisson, A. E. Santana, and J. C. da Silva, Int. J. Mod. Phys. A **20**, 4638 (2005).
[11] S. Kanemura and H.-T. Sato, Mod. Phys. Lett. A **10**, 1777 (1995).
[12] U. Wolff, Phys. Lett. B **157**, 303 (1985).
[13] K. G. Klimenko, Z. Phys. C **37**, 457 (1988).
[14] J. L. Kneur, M. B. Pinto, R. O. Ramos, and E. Staudt, Phys. Lett. B **657**, 136 (2007).
[15] B. Rosenstein, B. Warr, and S. H. Park, Phys. Rep. **205**, 59 (1991).
[16] Z. Bang-Rong, Commun. Theor. Phys. **47**, 695 (2007).
[17] T. W. Appelquist, M. Bowick, D. Karabali, and L. C. R. Wijewardhana, Phys. Rev. D **33**, 3704 (1986).
[18] Y. Nambu, Phys. Rev. **117**, 648 (1960); L. P. Gorkov, JETP **7**, 993 (1958).
[19] M. L. Bellac, *Thermal Field Theory* (Cambridge University Press, Cambridge, England, 1996).